Mechanism of Adsorption of Long-Chain Alkylamines on Silicates: A Spectroscopic Study. 2. Albite

ARTICLE *in* LANGMUIR · FEBRUARY 2001

Impact Factor: 4.46 · DOI: 10.1021/la001023u

3 AUTHORS, INCLUDING:

Irina V Chernyshova
Columbia University
41 PUBLICATIONS **691** CITATIONS
SEE PROFILE

Vidyadhar Ari
National Metallurgical Laboratory
43 PUBLICATIONS **255** CITATIONS
SEE PROFILE

Mechanism of Adsorption of Long-Chain Alkylamines on Silicates: A Spectroscopic Study. 2. Albite

I. V. Chernyshova,* K. Hanumantha Rao,† and A. Vidyadhar

Division of Mineral Processing, Department of Chemical and Metallurgical Engineering, Luleå University of Technology, SE-971 87 Luleå, Sweden

A. V. Shchukarev

Department of Inorganic Chemistry, Umeå University, SE-901 87 Umeå, Sweden

Received July 19, 2000. In Final Form: October 19, 2000

Using FTIR (DRIFTS and IRRAS) and XPS spectroscopy, ζ potential measurements, and Hallimond flotation tests, we confirmed that long-chain primary amines are adsorbed on silicates at pH 6−7 through the 2D−3D precipitation mechanism. The orientation and packing of dodecyl- and hexadecylammonium acetate and chloride adsorbed on albite in the different regions of the adsorption isotherm were determined. It was shown that these characteristics depend strongly on the substrate. Coadsorption of the counterion was not revealed, but the counterion was found to affect indirectly the adsorption at concentrations above the concentration of the bulk amine precipitation.

Introduction

Modification of the surface properties by adsorption of surfactants is exercised in numerous technologies.[1,2] In particular, primary long-chain alkylammonium salts (surfactants of weak electrolyte type) are most commonly used for beneficiation of silicates.[3] If the correlation between the oxide floatability and the precipitation of neutral molecules seems to be well established for alkaline pH,[4,5] at least at the macroscopic level, until recently, the adsorption of the amines at silicates at neutral pH has been explained mainly by the Gaudin−Fuerstenau model, which is known as the hemimicelle model.[6−9] This model postulates that amine cations are adsorbed in the outer Stern layer due to electrostatical attraction by negatively charged surface sites. At some threshold concentration the actual concentration of amine near the quartz surface becomes higher than the critical micelle concentration (CMC) and a two-dimensional (2D) process similar to ordinary bulk (3D) micellization takes place. As a result, the surfactant aggregates at the surface and its adsorption becomes appreciable. These 2D aggregates are called hemimicelles, and the critical concentration is referred to as the critical hemimicelle concentration (CHC). The hemimicelles are suggested to render the silicate surface hydrophobic due to exposing the hydrophobic chains toward the solution.

Less widespread was the condensation theory (CT) of Cases et al.,[10,11] which is the basis of the admicelle theory (AT) by Scamehorn et al.[12] The main idea of the CT is that the break in the adsorption isotherm at CHC corresponds to 2D condensation of the surfactant at the interface. It is assumed that such a 2D phase is chemically identical to either the 3D hydrated crystal or micelles of the surfactant at $T < T_K$ or $T > T_K$, respectively, where T_K is the Krafft point. The CT predicts that with a further increase in the bulk concentration the second layer (bilayer) can form through the tail−tail interactions and ascribes to this process the most pronounced vertical step in the adsorption isotherm. After that the bulk saturation (3D condensation) takes place.

However, as shown in our previous work,[13] the data obtained with the FTIR and XPS spectroscopies for quartz are inconsistent with the hemimicelle model, which cannot explain (1) the presence of the neutral amine molecules in the adsorbed film at below monolayer coverage and (2) a rather strong H-bonding between amino headgroups and the surface silanols. The CT, being more flexible, neglects the possibility of precipitation of long-chain amines at the interface also. To interpret the spectral dependences obtained for quartz, a model of successive

* To whom correspondence should be addressed at St. Petersburg State Technical University, Polytechnicheskaya 29, 195251 St. Petersburg, Russia. E-mail: Irina.Chernyschova@pobox.spbu.ru. Fax: +7 (812) 428-5712.

† E-mail: Hamumantha.Rao@km.luth.se.

(1) Ulman, A. In *An Introduction to Ultrathin Organic Films: From Langmuir−Blodgett to Self-assembly*; Academic Press: Boston, MA, 1991; pp 101−236.

(2) Riviere, J. C.; Mihra, S., Eds. *Handbook of Surface and Interface Analysis*; Marcel Dekker: New York, 1998.

(3) Leja, J. *Surface Chemistry of Froth Flotation*; Plenum Press: New York, 1982.

(4) Laskowski, J. S. *Challenges in Mineral Processing*; Sastry, K. V. S., Fuerstenau, M. C, Eds.; Society of Mineral Engineers: Littleton, CO, 1989; pp 15−34.

(5) Smith, R. W.; Scott, J. L. *Miner. Process. Extr. Metall. Rev.* **1990**, *7*, 81.

(6) Gaudin, A. M.; Fuerstenau, D. W. *Trans. Soc. Min. Eng. AIME* **1955**, *202*, 958.

(7) Somasundaran, P.; Fuerstenau, D. W. *J. Phys. Chem.* **1966**, *70*, 90.

(8) Novich, B. E.; Ring, T. A. *Langmuir* **1985**, *1*, 701.

(9) Fuerstenau, D. W.; Jang, H. M. *Langmuir* **1991**, *7*, 3138.

(10) Cases, J. M.; Mutaftschiev, B. *Surf. Sci.* **1968**, *9*, 57.

(11) Cases, J. M.; Villieras, F. *Langmuir* **1992**, *8*, 1251.

(12) Scamehorn, J. F.; Schechter, R. S.; Wade, W. H. *J. Colloid Interface Sci.* **1982**, *85*, 463.

(13) Chernyshova, I. V.; Rao, K. Hanumantha; Vidyadhar, A.; Shchukarev, A. V. *Langmuir* **2000**, *16*, 8071.

10.1021/la001023u CCC: $20.00
Published on Web 01/10/2001

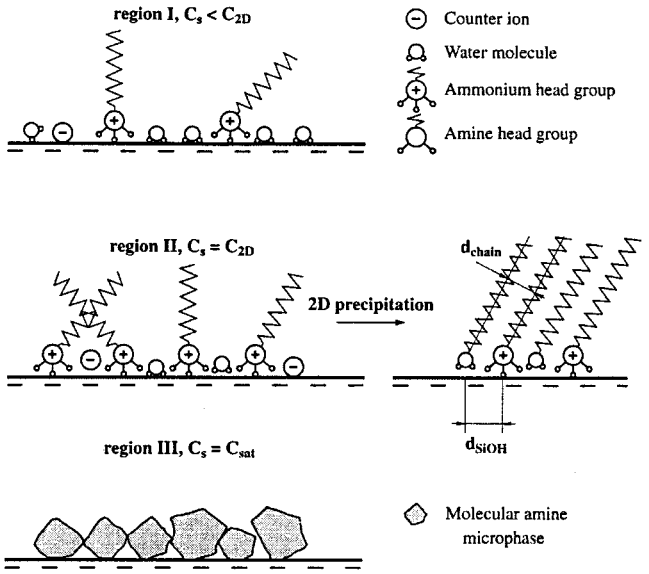

Figure 1. Scheme of the 2D−3D precipitation mechanism.

two-dimensional (2D) and three-dimensional (3D) precipitation of the long-chain amines was suggested. According to this model (Figure 1), before the transition to increased adsorption the ammonium headgroups are H-bonded to the negatively charged silanols as

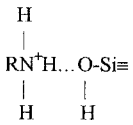

(1)

Due to electrostatic repulsion between the charged headgroups, the adsorbed amine ions are at large distances apart relative to the close-packed theoretical monolayer and the chains are chaotically oriented. When the local surfactant concentration at the interface approaches a critical value, the adsorbed layer transforms into crystalline state due to precipitation of neutral amine. At the first step, this process is two-dimensional and the adsorbed neutral amine establishes equilibrium.

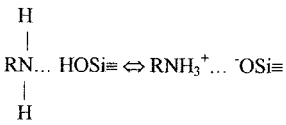

(2)

Screening the electrostatic repulsion between the headgroups, the neutral molecules change the structure of the adsorbed layer substantially, enhance the adsorption, and increase the density of the monolayer. The second phase transition (ordinary 3D precipitation) occurs when the bulk solubility limit is reached at the interface.

To confirm that the 2D−3D precipitation model is general in regard to the amine adsorption on the silicate surface, the focus of the present study was directed to study adsorption of acetate and chloride salts of hexadecyl and dodecyl alkylamines on albite ($NaAlSi_3O_8$). Feldspars (albite belongs to this common class) and quartz comprise more than 60% of the minerals at the earth surface. Of technological interest is separation of these minerals from each other. Therefore, elucidation the similarities and differences in interaction with the same reagent under the same conditions can help to find conditions under which the flotation response of these minerals differs. To solve this problem, the methodology developed in the previous paper[13] will be used. Namely, the concentration dependence of the DRIFTS spectra will be analyzed and correlated with ζ potential and flotation data measurement. The chemical identity, orientation, and packing of adsorbed species will be studied using the XPS and IRRAS methods.

Experimental Section

Reagents. Dodecylamine and hexadecylamine (HA) with purity of 99% were purchased from Fluka and Akzo Nobel, respectively. The acetate salts were synthesized by the standard procedure consisting in precipitation from the equimolar solutions of amine and acetic acid in benzene solvent. The amine acetate is insoluble in benzene below the freezing temperature, and it was purified thrice by recrystallization using fresh benzene each time. The XPS analysis (Table 1) reveals that nevertheless the acetate salts contain the molecular form, as an impurity. Solutions of DAAc and HAAc were prepared by dissolving the necessary

Table 1. XPS Characterization of Solid Amines, the Initial Fracture Surface of Albite, and the Albite Samples (Fracture Surface and Powder) Conditioned with the Amines

	element at. % (BE, eV)					
sample	N	C	O	Si	Al	Na
solid DA	4.65 (399.5)	89.36 (285.0) 0.07 (286) 0.02 (287.7)	2.58 (531.2)	0	0	0
solid DAAc	1.46 (399.4) 3.78 (401.1)	76.19 (285) 5.66 (286.9) 3.94 (288.4)	7.99 (531.2) 0.99 (533)	0	0	0
fresh fracture of natural albite	0	8.6 (285.0) 0.93 (286.4)	58.37 (532.2)	19.57 (103.0)	6.85 (74.7)	5.80 (1072.1)
fracture, 4×10^{-5} M DACl	0.12 (398.8) 0.65 (400.9)	22.6 (285.0) 1.33 (286.8)	48.36 (531.8)	18.92 (102.7)	6.29 (74.4)	1.75 (1071.8)
fracture, 4×10^{-5} M DAAc	0.5 (401.4)	13.71 (285.0) 0.94 (286.9)	54.76 (531.9)	20.30 (102.8)	6.47 (74.5)	3.31 (1071.9)
fracture, 2×10^{-4} M DAAc	0.17 (399.9) 0.39 (401.1)	27.08 (285.0) 1.62 (287.2)	47.03 (531.8)	18.34 (102.7)	6.01 (74.4)	0.68 (1071.7)
fracture, 2×10^{-4} M DACl	0.44 (399.7) 0.35 (401.3)	21.28 (285.0)	49.69 (531.9)	19.23 (102.8)	6.44 (74.4)	2.58 (1071.9)
fracture, 1×10^{-4} M HAAc	0.37 (399.6) 0.67 (401.5)	29.06 (285.0)	39.08 (531.7)	19.6 (102.6)	6.92 (74.2)	1.94 (1071.7)
powder, 1×10^{-5} M HAAc	0.61 (399.4) 0.61 (401.6)	30.87 (285.0) 2.74 (286.6)	44.44 (531.9)	14.91 (102.9)	5.04 (74.5)	0.76 (1072.0)

weight of the reagent in water. Naturally established pH was about 5.5, which then was adjusted by small quantities of NaOH. The solutions of DACl were prepared by continuous addition of the molecular amines and HCl into water so that the solutions were clear while pH was within the 6−7 range. Because HA is practically insoluble in water, it was first dissolved in ethanol. The stock aqueous solution of HAs contained 5% ethanol. Deionized water of specific conductance of 0.4−0.7 μS cm^{-1} was used in all experiments.

Materials. Natural polycrystalline (1−2-mm size crystals) albite of gray-white color supplied by the Mevior SS, Greece, was handpicked from their "Dasaki" feldspar deposit near Thessalonoki, Greece. The identity of the sample was verified by the XRD analysis. A plate with dimensions of about 20 × 20 mm^2 was cut from the polycrystal. The working surface was prepared by successive polishing with the SiC papers down to the 0.25 μm size and afterward thoroughly washed with deionized water. The XPS data on the fractured albite surface are shown in Table 1. The albite sample used in the present study was free from nitrogen impurity. To prepare powder the crystals were crushed, ground, and wet sieved to obtain the required size fractions (−5 μm and −150 + 38 μm). The finer size was obtained by microseiving in ultrasonic bath and employed for ζ potential measurements whereas the coarser size fraction was used for flotation tests. Specific surface areas (N_2-BET) was 0.15 and 2.78 m^2/g for the −150 + 38 μm and −5 μm fractions, respectively. ζ potential of the initial powder −5 μm size in deionized water at pH 6.5 was found to be −32 ± 2 mV.

Spectroscopic Characterization. The FTIR spectra were obtained with a Perkin-Elmer 2000 spectrometer at 4 cm^{-1} resolution with a narrow band liquid-N_2-cooled MCT detector. The IRRAS spectra were collected ex situ using an IRRAS accessory (Harrick, Inc.), by coadding 1000−1500 scans, both in *s*- and *p*-polarized radiation. To obtain the selected polarization, a wire-grid polarizer placed after the sample was used. The measurements were conducted immediately after 5 min conditioning of the quartz plate with the amine solution. The excess of the solution, if any, was removed carefully from the surface with a filter paper.

The DRIFT spectra were measured on the air-dried −5 μm powder after ζ potential measurements without mixing the samples with KBr. The untreated (initial) albite powder was used as reference. The DRIFTS Perkin-Elmer accessory was utilized. Each spectrum is average of 500 scans.

The XPS spectra were recorded with AXIS Ultra (Kratos) electron spectrometer under Al monoirradiation with sample cooling. Vacuum in sample analysis chamber during measurements was 10^{-8} Torr. The value of 285.0 eV was adopted as the standard C1s binding energy.

ζ potential measurements were made with a Laser Zee Meter, model 501, of Pen Kem, Inc., equipped with a video system. All experiments were conducted at a pH of 6−7 and at normal laboratory atmosphere and temperature (20 ± 2 °C). Initially, a series of 100 mL of water or amine solutions with defined concentration preset to pH 6.5 were taken in Erlenmeyer flasks. A 0.1 g amount of albite powder was added into each of the flasks, and the pH of the system was quickly adjusted to maintain the preset pH. The pH was measured with PHM 83 AUTOCAL pH meter (Radiometer Copenhagen) using a glass electrode calibrated with standard buffer solutions, also obtained from the same company. The mineral suspension was conditioned with magnetic stirrer for 1 h, during which time pH was monitored and adjusted if necessary to maintain the preset pH. The pH was adjusted by suitable concentration solutions of NaOH (for the solutions of amine acetates) or HCl (for the solutions of molecular amines). The mineral suspension was then filled into the ζ-meter rectangular cell. Upon application of suitable potential (generally 100 V), the ζ potential was recorded. After the measurement, the pH was again measured (if there was a large deviation, greater than ±0.5, to the preset pH 6.5, the measurement was discarded) and the suspension was filtered using Millipore filter paper (pore size 0.22 μm). Although the ionic strength of the solution was varied in the same range as the concentration of the amine (up to 10^{-2} M), this effect was found to be negligible on the ζ potential as compared to the effect of the amine precipitation. The solids were allowed to air-dry overnight at the room temperature, and the DRIFT spectra were recorded for all the air-dried samples after ζ-potential measurements.

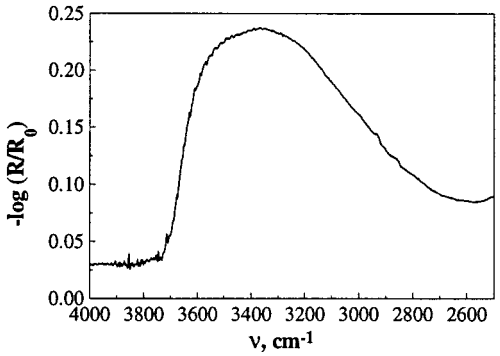

Figure 2. DRIFT spectra of initial albite measured against KBr.

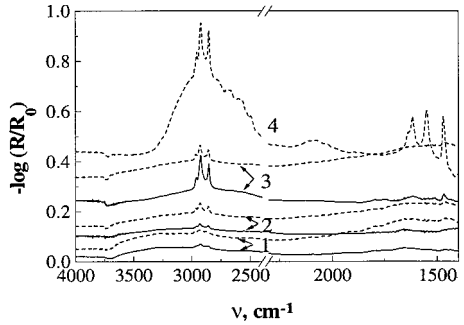

Figure 3. DRIFT spectra of albite powder (<5 μm size) after 1 h treatment with the DAAc (dashed lines) and DACl (solid lines) solution of the following concentration: (1) 5 × 10^{-6} M; (2) 1 × 10^{-4} M; (3) 1 × 10^{-3} M; (4) 1.5 × 10^{-2} M.

Flotation. The single mineral flotation tests were performed with a Hallimond flotation cell of 100 mL capacity. Initially, 1 g of the mineral was conditioned separately in 100 mL of predetermined concentration of amine solution and at given pH 6−7 for 5 min. The suspension was then transferred into the Hallimond cell for flotation for 1 min at the air flow rate of 8 mL/min.

Results

DRIFTS. Figure 2 shows the DRIFT spectrum of the initial −5 μm albite powder that was used as adsorbent. The H-bonded hydroxyls, which are predominantly attached to Si rather than Al surface atoms on the albite surface, and physically adsorbed water are responsible for the broad band centered at 3300 cm^{-1}.[14,15]

Figures 3 and 4 show selected spectra from a series of the DRIFT spectra of the albite powder conditioned with solutions of dodecyl- (DA) and hexadecylamonium (HA) of different initial concentration (C_b). All display the typical bands $\nu_{as}(CH_2)$ (∼2919 cm^{-1}), $\nu_s(CH_2)$ (∼2850 cm^{-1}), and $\nu_{as}(CH_3)$ (∼2955−2965 cm^{-1}) of alkyl chains. A broad band centered at ca. 3250−2800 cm^{-1} is attributed to the H-bonded $\nu(N^+H)$, ν(OH), and ν(NH) stretching vibrations. Similar to the case of quartz, the position of this band (3120 cm^{-1} for DACl and 3000 cm^{-1} for HACl before the break) is constant at concentrations below some critical value; after that the band shifts twice abruptly toward the red side, as illustrated by Figures 5, 6A, and 7A. This shift points to the strengthening of the H-bonding of amine headgroups. Since the band shifts down to 2900 cm^{-1},

(14) Kubicki, J. D.; Blake, G. A.; Apiz, S. E. *Am. Mineral.* **1996**, *81*, 789.

(15) Coretsky, C. M.; Sverjensky, D. A.; Salisbury, J. W.; D'Aria, D. M. *Geochim. Cosmochim. Acta* **1997**, *61*, 2193.

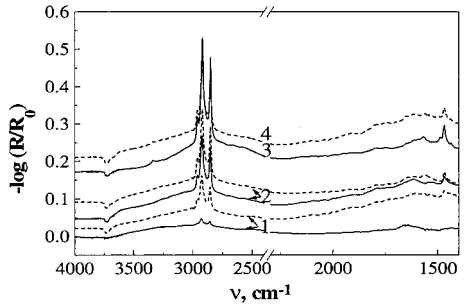

Figure 4. DRIFT spectra of albite powder (<5 μm size) after 1 h treatment with the HAAc (dashed lines) and HACl (solid lines) solution of the following concentration: (1) 2×10^{-6} M; (2) 2×10^{-5} M; (3) 5×10^{-5} M; (4) 4×10^{-5} M.

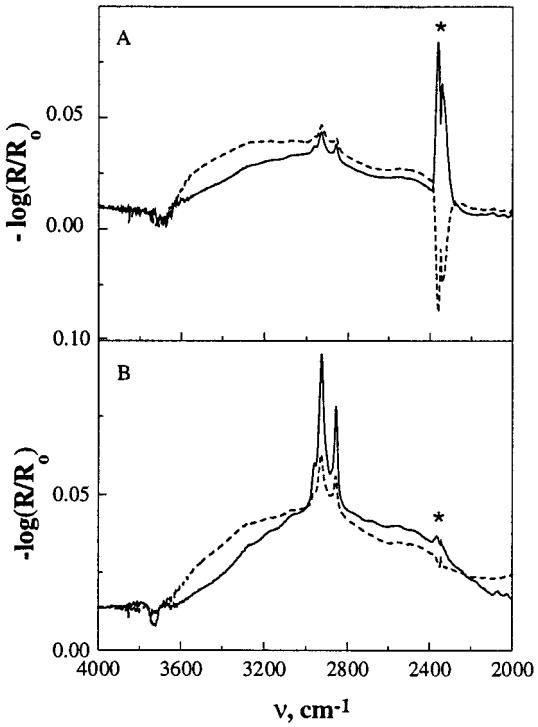

Figure 5. DRIFTS spectra of albite conditioned with (A) DACl at 2×10^{-5} M (solid line) and 5×10^{-5} M (dashed line) and (B) HACl at 2×10^{-6} M (solid line) and 5×10^{-6} M (dashed line). Asterisks indicate uncompensated absorption by atmosphere CO_2.

this observation is not obscured by a possible variation in the quantity of physically adsorbed water, which is characterized by the broad absorption at ca. 3300 cm^{-1} (Figure 2).

In the DRIFTS spectra of the albite conditioned with solutions of C_{16} amines of concentration higher than 4×10^{-5} M (Figure 4), new bands at 3330, 1650−1640, 1570, and 1490 cm^{-1} become distinct. From comparison with the transmission spectrum of bulk (3D) phase of the molecular HA (Figure 8) (see for assignment Table 2), we concluded that at $C_b > 4 \times 10^{-5}$ M bulk HA amine precipitates. At the same time, in the case of the C_{12} amines the 3330 cm^{-1} band does not appear even at the concentration as high as 1.5×10^{-2} M (DAAc), which is distinct from the case of quartz.[13] Since the XPS spectra (vide infra) revealed the presence of the molecular form, this discrepancy can be attributed to another packing of the DA precipitates in the case of albite, possibly due to incorporation of the ionic amine.

All the DRIFT spectra exhibit the negative double band at 3725−3737 cm^{-1} with full width at half-

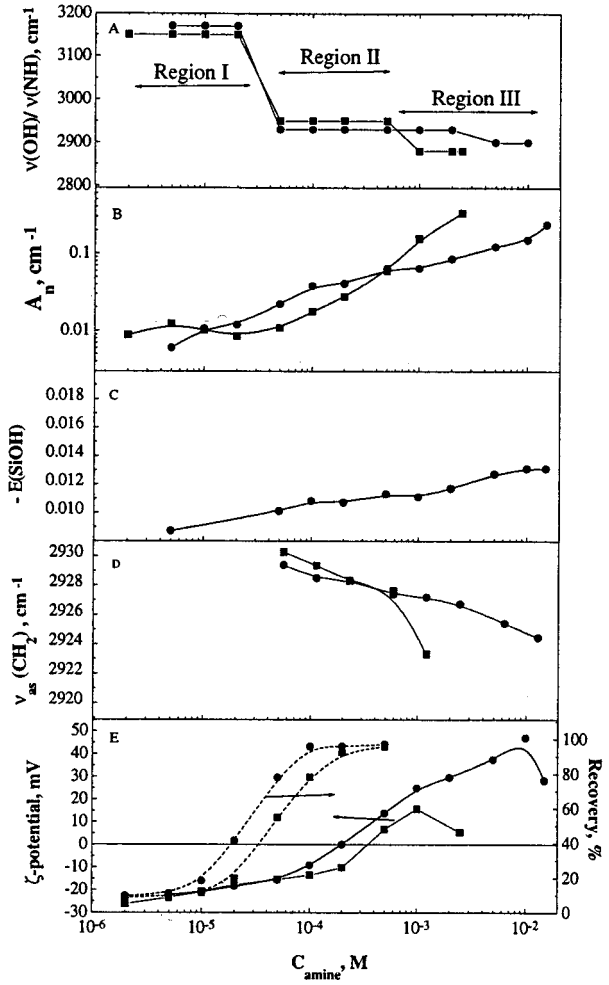

Figure 6. Absorption characteristics of DAAc (circles) and DACl (squares) as functions of the concentration at pH 6−7 and $t = 20$ °C: (A) position of the "H-bonded" band of the ν(OH), ν(NH), and $\nu(N^+H)$ vibrations; (B) normalized integrated intensity $A_n = A/11$, cm^{-1}, of the $\nu_{as}(CH_2)$ band; (C) peak intensity of the absorption band at 3740 cm^{-1} of the silanol groups; (D) frequency of $\nu_{as}(CH_2)$; (E) ζ potential (solid lines) and flotation recovery (dashed lines).

maximum (fwhm) = 35 cm^{-1}. This band is positioned at a lower frequency and is much broader as compared to that of free silanols on albite (3740−3742 cm^{-1}, fwhm = 5 cm^{-1} [14]). Although the hydrogen perturbed and geminal silanols absorb in this region,[16] we assign the band in question to the free silanols on the non-stoichiometric albite surface, from which Na^+ cations are dissolved. The removal of Na^+ cations during conditioning with water was detected with the XPS method (not shown). This assignment agrees with the ab initio study,[17] according to which the removal of the charge balancing Na^+ cations will increase the net negative surface charge, which decreases the frequency of the ν(O−H) band. The negative intensity of the ν(SiO−H) band results from the interaction of silanols (probably via H-bonding) with the absorbed amine. The fact that the specific interaction of the amine (ammonium) headgroups and silanols is rather significant follows from a comparison of the DRIFTS spectra of DACl adsorbed from the 2×10^{-4} M solution at pH 2 (pzc) and 6.5 (Figure 9).

(16) Vansant, E. F.; Van Der Voort, P.; Vrancken, K. C. *Characterisation and Chemical Modification of the Silica Surface*; Elsevier: Amsterdam, 1995.

(17) Kubicki, J. D.; Blake, G. A.; Apiz, S. E. *Am. Mineral.* **1996**, *81*, 789.

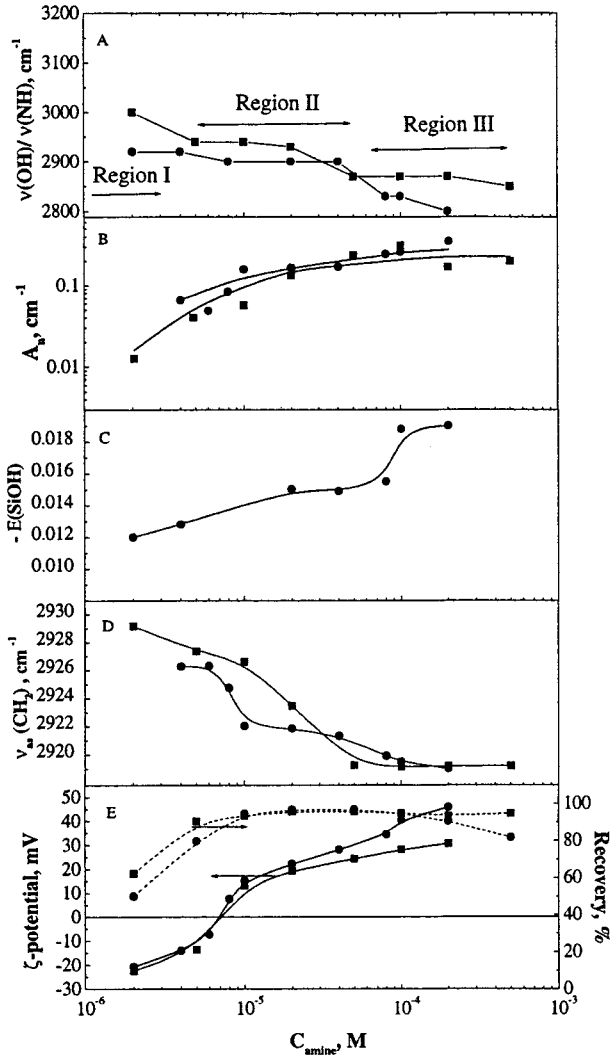

Figure 7. Absorption characteristics of HAAc (circles) and HACl (squares) as functions of the concentration at pH 6−7 and $t = 20$ °C: (A) position of the "H-bonded" band of the ν(OH), ν(NH), and ν(N^+H) vibrations; (B) normalized integrated intensity $A_n = A/15$, cm^{-1}, of the $\nu_{as}(CH_2)$ band; (C) peak intensity of the absorption band at 3740 cm^{-1} of the silanol groups; (D) frequency of the $\nu_{as}(CH_2)$; (E) ζ potential (solid lines) and flotation recovery (dashed lines).

One can see that the quantities of the adsorbed amine are almost the same. It is worth noting that the position of the "H-bonded" band is different: at 3200 cm^{-1} at pH 2 and at 2950 cm^{-1} at pH 6.5 (see below for discussion).

The normalized intensity of the $\nu_{as}(CH_2)$ band, A_n, which was calculated as the band absorbance integrated within the 2945−2902 cm^{-1} range and divided by the number of the methylene units in the chain, is proportional to the surface coverage. The number of the reacted surface silanol groups is assumed to be proportional to the peak intensity, E, of the negative 3737−3725 cm^{-1} band. Quantities A_n and E as functions of the amine concentration are plotted in Figures 6 and 7 (for DA and HA, respectively), along with the concentration dependences of frequencies of the $\nu_{as}(CH_2)$ and "H-bonded" bands. Inspection of these dependences reveals the following:

(1) The break in the A_n dependences coincides with the first red shift of the "H-bonded" band and with the steep decrease in $\nu_{as}(CH_2)$. Therefore, the enhancement of the amine adsorption occurs simultaneously with a strengthening of the H-bonding and an increase in the chain order. As in the case of quartz, this effect can be associated with

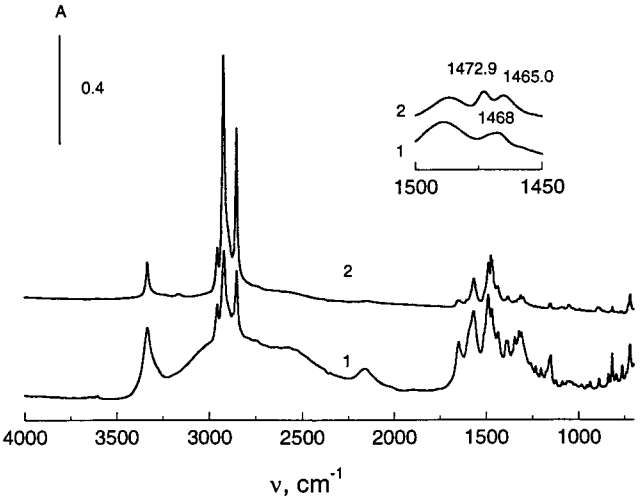

Figure 8. (1) DRIFT spectrum of C_{12} amine in KBr matrix and (2) transmission spectra of thick polycrystalline films of C_{16} amine deposited on a KBr plate from the solutions in ethanol. The insert shows the enlarged region of the $\delta(CH_2)$ vibrations.

2D precipitation of molecular amine, whose formation is detected with the XPS spectra (vide infra). The critical concentration at which these spectrum changes are observed is denoted as C_{2D}

(2) The second jump in the position of the "H-bonded" band is observed for all the amines (Figures 6A and 7A). Being accompanied in the case of the HAs by the appearance of the 3330 cm^{-1} characteristic of the bulk molecular amine, this jump can be due to the 3D precipitation which change H-bonds of amino groups.

(3) The plateau of the E curves (occupation of all available surface silanols by the adsorbed amine) is reached at a concentration close to the upper limit of the concentration range under study, which in the case of HAs is much higher than the concentration of bulk precipitation, C_{3D} (ca. 4×10^{-5} M). It follows that the adsorption of the HAs at the fine albite powder is highly inhomogeneous: even at the concentration as high as C_{3D} a part of the surface is still bare, which confirms the patchlike regime of the adsorption.[13]

XPS. The XPS measurements were conducted at the fracture and powder albite. The results are shown in Figures 10 and 11 and Table 1.

Adsorption of the amines manifests itself in the XPS spectra by (1) appearance of the N 1s signal of the amino groups, (2) the 1.5−3.5-fold increase in the intensity of the C 1s peak as compared to that of the initial surface (Table 1), (3) a decrease in the peak intensities of Si, O, and Al, due to screening the mineral surface by the adsorbed amine, and (4) a decrease of the peak of Na, which is caused by dissolution of sodium cations during the conditioning of the samples with the amine solutions. In contrast to the case of quartz, the coadsorption of chlorine and acetate counterions was not detected.

Similar to quartz, the N 1s spectrum of the albite conditioned 10 min in the 4×10^{-5} M solutions of the DA consists of a single peak at 401.4 eV in the case of DAAc (Figure 10) and a peak at 400.9 eV with a small satellite at 398.8 eV in the of case DACl (Figure 11), while at a higher concentration (2×10^{-4} M) two N 1s peaks at 399.8 $\pm$ 0.1 and 401.2 $\pm$ 0.1 eV are present. The two peaks also characterize the layer adsorbed at the powder and the fracture from respectively the 1×10^{-5} M and 1×10^{-4} solutions of HAAc (Table 1). In a comparison of these BE values with those of amino and ammonium groups (Table 1) and using the same arguments as in the case of quartz,[13]

Table 2. Assignment of the Major Absorption Bands of DA and DAAc in Solid Form[a]

$C12H23NH2$		$C12H23NH3+Ac-$	
ν, cm^{-1}	mode	ν, cm^{-1}	mode
3333	$\nu_{as}(NH_2) + \nu_s(NH_2)$ NH···N H-bonded	~3000 (broad)	$\nu_{as}(NH_3^+)$
		~2600 (broad)	$\nu_s(NH_3^+)$
2956	$\nu_{as}(CH_3)$	2963	$\nu_{as}(CH_3)$ (Ac^-)
2920	$\nu_{as}(CH_2)$	2950	$\nu_{as}(CH_3)$
2873	$\nu_s^{in}(CH_3)$	2933	$\nu_{as}(CH_3)$ (Ac^-)
2852.5	$\nu_s(CH_2)$	2921.6	$\nu_{as}(CH_3)$
2800 (broad)	ν(OH···N) water contamination	2900	$\nu_s(CH_2)$ FR[b]
		2890	$\nu_s(CH_2)$ FR[b]
		2870.7	$\nu_s^{in}(CH_3)$
		2851.6	$\nu_s(CH_2)$
1650	$\delta_{as}(NH_2) + \delta(H_2O)$	1645	ν_{as}(COO) (Ac^-) + $\delta(H_2O)$
1570	$\delta_s(NH_2)$	1544	$\delta_{as}(NH_3^+) + \delta(H_2O)$
1490	?	1520	$\delta_s(NH_3^+)$
1470	$\delta(CH_2)$	1460−1480	$\delta(CH_2)$
1388	$\omega(CH_2)$	1407	ν_s(COO) (Ac^-)
1153	$\rho(NH_2)$	1337	
		1010	$\rho(CH_3)$ (Ac^-)
		920	ν(CC) (Ac^-)

[a] Ihs, A.; Liedberg, B.; Uvdal, K.; Tornkvist, C.; Bodo, P.; Lundstrom, I. *J. Colloid Interface Sci.* **1990**, *140*, 192. Bellamy, L. J. *The Infrared Spectra of Complex Molecules*; Wiley: New York, 1975. Przeslawska, M.; Melikowa, S. M.; Lipkowski, P. *Vib. Spectrosc.* **1999**, *20*, 69. [b] FR = Fermi resonance components of the band coupling with overtone of $\delta(CH_3)$.

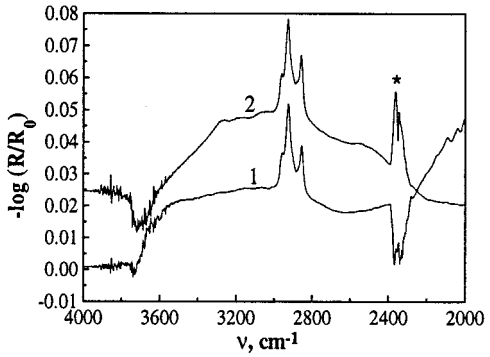

Figure 9. DRIFT spectra of albite powder conditioned in the 2×10^{-4} M DACl solution: (1) 10 min at pH 2; (2) 1 h at pH 6.05.

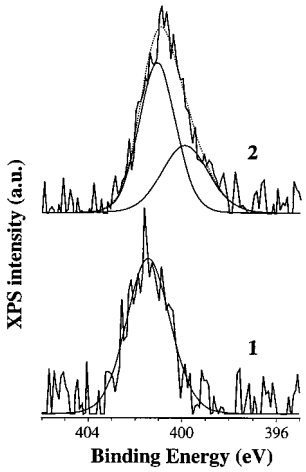

Figure 10. XPS N 1s spectra of a fracture albite surface conditioned in a solution (pH 6.5) of DAAc. The amine concentration is (1) 4×10^{-5} M and (2) 2×10^{-4} M.

the single (principle) peak at 401.4 eV (400.9 eV) can be assigned to the nitrogen in the moiety of eq 1, while the doublet can be assigned to the equilibrium eq 2, where the peak with the BE 399.8 ± 0.1 eV corresponds to the neutral amine in the left part of the eq 2. However, the BE for the ammonium group attached to the albite surface before the precipitation (401.4−400.9 eV)

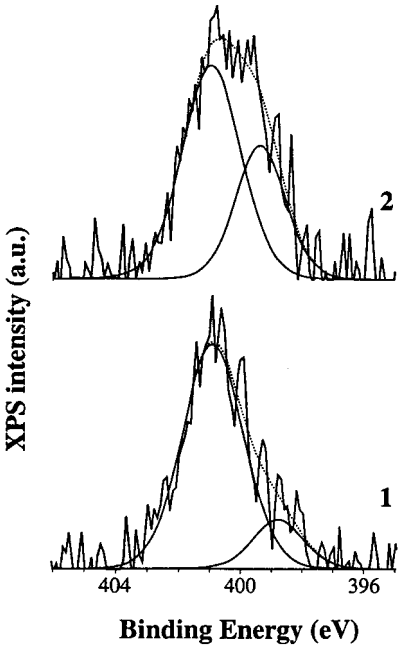

Figure 11. XPS N 1s spectra of a fracture albite surface conditioned in a solution (pH 6.5) of DACl. The amine concentration is (1) 4×10^{-5} M and (2) 2×10^{-4} M.

is higher by ca. 1 eV as compared to that for quartz (400.1 eV). This difference can be attributed to the preferential initial adsorption of the protonated amine at the sodium vacances and, if at the silanol oxygen, to the enhanced proton-accepting capability of the surface silanols in the vinicity of such a vacation. It is interesting that the doublet position for the albite and quartz is the same within the experimental error, which implies that the second step of the amine adsorption mechanism (eq 2) is probably similar.

IRRAS. Figures 12−15 show the *s*- and *p*-polarized IRRAS spectra the albite surface conditioned 5 min in the solutions of the acetate and chloride salts of HA and DA. The spectra were measured at the angles of incidence in the 70−80° range. The choice of this angle will be justified below. The differences with the DRIFTS spectra are as follows.

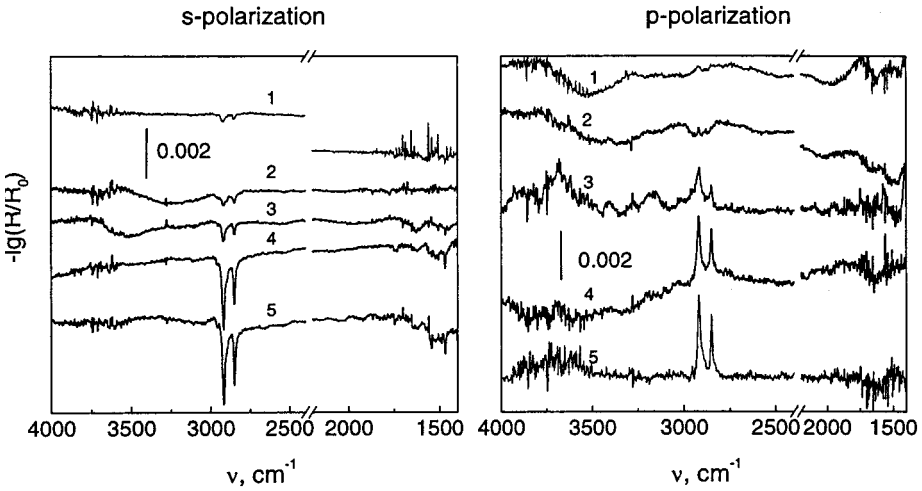

Figure 12. IRRAS spectra of amines adsorbed on an albite surface. *s*-polarized spectra are shown on the left, and *p*-polarized spectra, on the right. Key: (1) DAAc at 2×10^{-5} M; (2) DAAc at 1×10^{-4} M; (3) HACl at 2×10^{-5} M; (4) HACl at 1×10^{-4} M; (5) HAAc at 1×10^{-4} M. The angle of incidence is 80°.

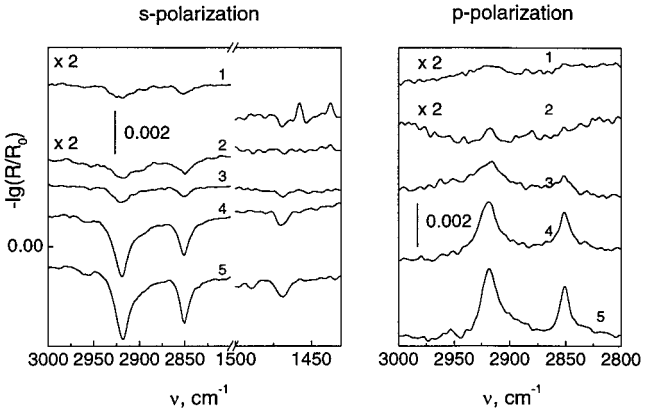

Figure 13. Enlargement of Figure 12 in the 3000−2800 and 1500−1400-cm^{-1} regions. Note that spectra 1 and 2 are multiplied by a factor of 2.

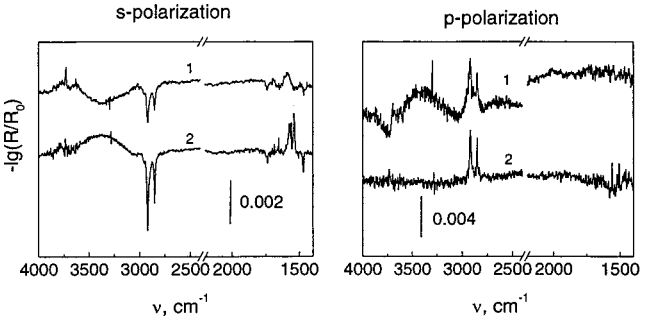

Figure 14. IRRAS spectra of amines adsorbed on an albite surface. *s*-polarized spectra are shown on the left, and *p*-polarized spectra, on the right. Key: (1) HAAc at 2×10^{-5} M, angle of incidence 70°; (2) HACl at 1×10^{-4} M, angle of incidence 73°.

(1) In general for any film on any transparent substrate, the absorption bands in the *s*-polarized spectra are negative. This is caused by the so-called "optical effect"[18] (the negative direction of the *s*-polarized reflection−absorption band is reproduced by the spectrum simulation using the Fresnel formulas).

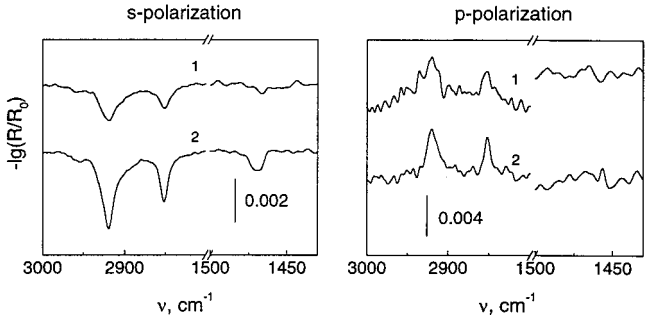

Figure 15. Enlargement of Figure 14 in the 3000−2800 and 1500−1400-cm^{-1} regions. Note that spectra 1 and 2 are multiplied by a factor of 2.

(2) Due to the optical effect, the *p*-polarized spectrum of a film on a transparent substrate is always the superposition of two spectra, the spectrum of the modes that have components of the transition dipole moments (TDM) perpendicular to the surface and the spectrum of the modes whose TDMs are directed along the surface. According to optical theory,[19,20] at the angle of incidence greater than the Brewster angle ($\varphi_{Br} \approx 58.3°$), the "perpendicular" bands point downward, while the "parallel" bands point upward.

(3) There is an additional band at 1740−1750 cm^{-1}, where carbonyl groups absorb. In some cases this band disappeared after washing of the sample with water. On the basis of XPS spectra, in which carbonyl was not detected, we assigned it tentatively the band to coadsorbed carbonate which evaporates in the XPS chamber.

(4) The directions of the broad intensive absorption bands in the 3300−3500 cm^{-1} region for DA (Figure 12, curves 1 and 2) and HA at 2×10^{-5} M (Figure 12, curve 3, and Figure 14, curve 1) testify to coadsorpion of molecular water, while for HA at 1×10^{-4} M (Figure 12, curves 4 and 5, and Figure 14, curve 2) the water adsorbed during the surface preparation is squeezed out by the adsorbed amine.

(5) The $\delta(CH_2)$ band around 1465−1470 cm^{-1} in the *s*-polarized spectra of the HAs can be distinguished for

(18) Horn, A. *Spectroscopy for Surface Science*; Clark, R. J. H., Hester, R. E., Eds.; John Wiley and Sons: New York, 1998; Vol. 26, pp 273−339.

(19) Hoffmann, H.; Mayer, U.; Krischanitz, A. *Langmuir* **1995**, *11*, 1304.

(20) Brunner, H.; Mayer, U.; Hoffmann, H. *Appl. Spectrosc.* **1997**, *51*, 209.

Table 3. Characteristics of the Adsorded Layers, Taken from the IRRAS Spectra Shown in Figures 13 and 15

soln	angle of incidence (deg)	$\nu_{as}(CH_2)^s$ [a] (cm^{-1})	$\nu_s(CH2)^s$ (cm^{-1})	DR_{asym}	DR_{sym}	γ and ϕ, calcd from DRs (deg)	$(A_{as}/A_s)^s$	$(A_{as}/A_s)^s$	ϕ calcd from $(A_{as}/A_s)^s$ (deg)	no. of monolayers[b]
HACl, 1×10^{-5} M	70	2919.2	2850.9	−0.33	−0.34	0, uni[c]	1.50			0.75
HAAc, 2×10^{-5} M	80	2919.6	2850.2	−0.54	−0.55	0, uni	1.60	1.63		0.72
HACl, 1×10^{-4} M	73	2919.7	2851.6	−0.76	−0.59	45, 39	1.60	1.26	41	2.3
HACl, 1×10^{-4} M	80	2918.9	2850.8	−1.11	−0.93	46, 41	1.64	1.37	41	3.6
HAAc, 1×10^{-4} M	80	2918.3	2850.8	−1.00	−0.84	43, 42	1.59	1.35	41	4.1
DAAc, 2×10^{-5} M	80	2921.0	2853.0	−1.65		iso	1.30			0.54
DAAc, 1×10^{-4} M	80	2919.6	2850.2	−1.3		52	1.12			0.82

[a] The band position in the *s*-polarized spectrum. [b] Estimation of the number of monolayers was done with $k_{max} = 1.04$ for HAs and 0.62 for Das. [c] Uniaxial symmetry.

analytical purposes (Figures 13 and 15). Although this band is single in all the cases, the position of its maximum varies from one spectrum to another. The films adsorbed from the 1×10^{-4} M HA solutions are characterized by the band centered around 1469−1470 cm^{-1}, while the band at 1467−1468 cm^{-1} is observed in the *s*-polarized spectrum of the film formed at 2×10^{-5} M. It has been established[21,22] that the single broad (fwhm ∼ 10−11 cm^{-1}) band at ca. 1466 cm^{-1} is characteristic of a relatively disordered hexagonal subcell where the hydrocarbon chain freely rotates around its long axis. This subcell has uniaxial symmetry. Excepting a triclinic (most dense) subcell, which is characterized by a sharp, narrow, and single band at 1471 cm^{-1},[23] the $\delta(CH_2)$band is split into a doublet in biaxial subcells: the doublet components are 1473 and 1463 cm^{-1} for an orthorhombic perpendicular subcell, and the splitting is 5−8 cm^{-1} in the case of an orthorhombic inclined (∼30°) subcell. The splitting is also expected[21,22] for molecular packing in the monoclinic (∼30° tilt) subcell. For illustration, the insert in Figure 8 shows the $\delta(CH_2)$ bands of DA and HA. In the case of DA this band is single and broad with the maximum at 1468 cm^{-1}, while for hexadecylamine it is split into two components at 1472.9 and 1465.0 cm^{-1}. Since melting points of DA and HA are about 28 and 43 °C,[24] respectively, it is likely that DA is in amorphous state while HA is packed in a orthorhombic or monoclinic cell. Keeping the above correlations in mind, one can suppose that HA adsorbed at 2×10^{-5} M is in a liquidlike state or packed in a hexagonal subcell, while at the high concentration the symmetry of the packing becomes higher, which is responsible for the higher band frequency. The fact that the splitting is not observed in the latter case can be attributed to the mixed (domainlike) composition of the adsorbed film.

The above qualitative differentiation of the packing modes of the adsorbed amines is in agreement with the frequencies of the methylene stretching bands:[25,26] $\nu_{as}(CH_2) < 2919$ cm^{-1} in the case of HAs adsorbed at 1×10^{-4} while in the other cases $\nu_{as}(CH_2) > 2919$ cm^{-1} (Table 3). Moreover, the relatively high intensity of the $\nu_{as}(CH_3)$ band at 2967 cm^{-1} in the *s*-polarized spectra of adsorbed DAs as compared to that of the adsorbed HAs (Figures 12−15) and the presence of the distinct positive band $\nu_s^{in}(CH_3) \approx 2878$ cm^{-1} in the *p*-polarized spectrum, along with the larger bandwidths, point to a rather high percent of fractional population of gauche conformations for the adsorbed DAs.[27] In addition, in the latter case the band $\nu_s(CH_2^{FR})$ (FR ≃ Fermi resonance) at 2898 cm^{-1} is more intensive than that of well-packed amphiphiles (see Figures 13 and 15 and the spectra in refs 21, 25, 26, and 28), which can also be ascribed to the loose packing of the DAs.

To calculate the molecular orientation (MO) in the adsorbed layers, the following procedure[29] was employed. One can simulate the absorbance of the monolayer in the IRRAS spectra by the linear-approximation expressions derived by Mielczarski:[30]

$$A_{s(y)} \approx -\frac{16\pi}{\ln 10}\left[\frac{\cos \varphi_1}{n_3^2 - 1}\right]\frac{n_{2y}k_{2y}d_2}{\lambda} \tag{3}$$

$$A_{p(x)} \approx -\frac{16\pi}{\ln 10}\left[\frac{\cos \varphi_1}{\xi_3^2/n_3^4 - \cos^2 \varphi_1}\right]\left[-\frac{\xi_3^2}{n_3^4}\right]\frac{n_{2x}k_{2x}d_2}{\lambda}$$

$$A_{p(z)} \approx -\frac{16\pi}{\ln 10}\left[\frac{\cos \varphi_1}{\xi_3^2/n_3^4 - \cos^2 \varphi_1}\right]\frac{\sin^2 \varphi_1}{(n_2^2 + k_2^2)^2}\frac{n_{2z}k_{2z}d_2}{\lambda}$$

where φ_1 is the angle of incidence, $\xi_3 \equiv (\hat{n}_3^2 - \sin^2 \varphi_1)^{1/2}$ is the generalized complex refractive index of the substrate, and n_3 is the refractive index of the substrate. The quantities n_{2i} and k_{2i} ($i = x, y, z$; the direction of the *z* axis in the laboratory system is assumed to be perpendicular to the film surface, and the *y* axis is directed along the electric field vector of the *s*-polarized radiation) are respectively the principle values of the refractive and absorption indices of the anisotropic film. These values strongly depend on the packing and orientation of molecules in the film. For the methylene stretching vibrations in the uniaxially distributed hydrocarbon chains the principle components of the absorption index are given by

$$k_{2x} = k_{2y} = k_{max}\frac{\cos^2 \gamma + 1}{4} \tag{4}$$

where γ is the average tilt angle and k_{max} is the absorption

$$k_{2z} = k_{max}\frac{\sin^2 \gamma}{2}$$

coefficient of the $\nu(CH_2)$ band of a hypothetical sample in which the density of the chains is the same as in the film

(21) Flach, C. R.; Gericke, A.; Mendelsohn, R. *J. Phys. Chem. B* **1997**, *101*, 58.
(22) Snyder, R. G. *J. Mol. Spectrosc.* **1961**, *7*, 116.
(23) Holland, R. F., Nielsen, J. R. *J. Mol. Spectrosc.* **1962**, *9*, 436.
(24) Ash, M.; Ash, I. *Handbook of Industrial Surfactants*; Gower Publishing Co.: Aldershort, England, 1993.
(25) Mendelsohn, R.; Brauner, J. W.; Gericke, A. *Annu. Rev. Phys. Chem.* **1995**, *46*, 305.
(26) Gericke, A.; Huhnerfuss, H. *J. Chem. Phys.* **1993**, *97*, 12899.
(27) Brinner, H.; Vallant, T.; Mayer, U.; Hoffmann, H. *Surf. Sci.* **1996**, *368*, 279.
(28) Sakai, H.; Umemura, J. *Langmuir* **1998**, *14*, 6249.
(29) Chernyshova, I. V.; Rao, K. Hanumantha *J. Phys. Chem. B*, in press.
(30) Mielczarski, J. A.; Yoon, R. H. *J. Chem. Phys.* **1989**, *93*, 2034.

under study but all TDMs of the equivalent chains are codirected. For the same vibrations in a biaxial film

$$k_x = k_{max}(1 - \cos^2\gamma \sin^2\phi)$$
$$k_y = k_{max}(1 - \sin^2\gamma \sin^2\phi) \quad (5)$$
$$k_z = k_{max} \sin^2\gamma$$

where ϕ is the azimuth angle. The values of the real part of the refractive index can be expressed analogously.[31]

The method used for evaluation of the MO involves measuring the dichroic ratio (DR) from the experimental IRRAS spectra. Here, the DR is defined as the ratio of the peak intensity of the absorption band in the *s*-polarized spectrum, A_s, to that in the *p*-polarized spectrum, A_p:

$$DR = \frac{A_s}{A_p} = \frac{A_y}{A_x + A_z} \quad (6)$$

The experimental value of DR is fitted with the theoretical one calculated using eqs 3 with k_{2i} represented by either eqs 4 or 5 depending on the film symmetry. In doing so, one excludes the thickness from the MO measurements and reduces the error produced by the uncertainty in k_{max}. This is important advantage of the procedure since there is no way to determine these parameters correctly in practice.

Since the layer deposition is not precisely reproducible and the amount of the adsorbed species under study is low (of the order of a monolayer), the IRRAS spectra cannot be measured for the same sample at several angles of incidence, which could increase the accuracy of the results. Instead, the *s*- and *p*-polarized spectra are measured at one angle of incidence, which is optimum from the viewpoints of the signal-to-noise ratio (SNR), sensitivity to an orientational change, and resistance in regard to the uncertainty in k_{max} and n_{2i}. To determine this angle we first measured the refractive index of the albite plate. For this purpose, IRRAS spectra of the plate were recorded at several angles of incidence within the 60−80° range, using the IRRAS spectra taken at 80° as reference. With variation of the refractive index of the substrate, the experimental reflectivities were fitted with those simulated with the Fresnel formulas for the two-phase system.[32] The best fit corresponds to $n = 1.62$. Using this value we simulated the angle-of-incidence dependence of the band depth, ΔR, in the IRRAS spectra of a model anisotropic film 2.13 nm thick and found that the angular angle of 73−80° is optimal for the orientational measurements.

The algorithm of the MO measurements consisted in the following steps:[29]

(1) The *s*- and *p*-polarized IRRAS spectra were obtained at the optimum angle of incidence (in the 73−80° range), from which the DRs for the $\nu_{as}(CH_2)$ and $\nu_s(CH_2)$ bands (DR_{as} and DR_s, respectively) were calculated.

(2) The values of DR_{as} and DR_s were used for discriminating between the uniaxial and biaxial packing of the chains: if $DR_{as} = DR_s$ within the standard deviation of the statistical group, the symmetry of the layer is assumed to be uniaxial and the tilt angle is determined from function $DR(\gamma)$ simulated by using eqs 3 and 4. If $DR_{as} \neq DR_s$, the film is assumed to be biaxial and the averaged value $DR_{av} = {}^1/_2(DR_{as} + DR_s)$ is calculated. This value is used for determining the tilt angle from the "uniaxial" function $DR(\gamma)$ above-mentioned.

(3) With utilization of the value of the tilt angle obtained at the previous step, the azimuth angle ϕ is obtained by fitting the experimental DR and/or the ratio of the peak intensities of the $\nu_{as}(CH_2)$ and $\nu_s(CH_2)$ bands in the *s*-polarized spectra, $(A_{as}/A_s)_s$, by the corresponding values simulated respectively with eqs 3 and 5 and the function

$$\left(\frac{A_{as}}{A_s}\right)_s = \frac{k_{max,as}}{k_{max,s}} \frac{1 - \sin^2\gamma \sin^2\phi}{1 - \sin^2\gamma \cos^2\phi} \quad (7)$$

where A_{as} and A_s and $k_{max,as}$ and $k_{max,s}$ are respectively the peak intensities in the *s*-polarized spectrum and the maximal absorption indices of $\nu_{as}(CH_2)$ and $\nu_s(CH_2)$. In the approach using $(A_{as}/A_s)_s$ the value of $k_{max,as}/k_{max,s}$ is needed. Assuming that the crystallites formed by drying a drop of a highly concentrated solution of hexadecylamine in ethanol on a KBr plate are randomly oriented, we obtained $k_{max,as}/k_{max,s} = 1.5$ from the transmission spectrum of these crystallites (Figure 8, curve 2).

To measure the MO, the auxiliary plots were constructed (not shown) for the experimental DRs and the optical configurations used. The optical parameters $n_{2x} = n_{2y} = 1.49$, $n_{2z} = 1.55$, and $k_{2max} = 1.04$ reported for the $\nu_{as}(CH_2)$ band of 11 monolayer CdAr Langmuir−Blodgett films on glass[33] were adopted.

It follows from the experimental values of DR (Table 3) that the hydrocarbon chains of HAs adsorbed at 2×10^{-5} M take a uniaxial perpendicular orientation (this result was reproduced in several experiments). In view of the features of the $\delta(CH_2)$ band discussed above, it is likely that chains are packed in a perpendicular hexagonal subcell. The biaxial arrangement of the HAs adsorbed at 1×10^{-4} M (the biaxiality is 5° from the magic angle (45°)) indicates that the chains are more well-ordered as compared to the former case. The higher frequencies of the $\delta(CH_2)$ bands support this conclusion. Notice that the values of the azimuth angle obtained employing both the DR and $(A_{as}/A_s)_s$ values are in good agreement with one another, testifying to the adequacy of the biaxial model and the value $k_{max,as}/k_{max,s} = 1.5$, which were chosen for the MO calculations. At the same time, the average tilt angle (43−46°) of the chains in the biaxial films is high. Taking into account that the layer coverage is more than one monolayer (Table 3; vide infra) and the fact[34] that in the close-packed state of the hydrocarbon chains the tilt angle is 0 or 30°, we suggest that the biaxial film is composed mostly from well-packed clusters randomized at the surface (in the case of the full isotropy the average tilt angle would be ≈55°). This assignment is consistent with the 3D precipitation mechanism of formation of these films. Since the albite surface is polycrystalline, the biaxiality can originate also from the molecule distribution with a preferred twist angle and isotropic azimuth angle.[35] In the context of the present study, in virtue of the low biaxial anisotropy, we did not consider this possibility.

The band intensities in the *p*-polarized spectra of DA films are dramatically weaker than those of the HA films (Figure 12). Therefore, the quantitative information includes a higher uncertainty. Nevertheless, we inferred that DA species adsorbed at 2×10^{-5} M are in liquidlike (isotropic) phase, while at 1×10^{-4} M they are partially

(31) Dunmur D.; Toriyama, K. In *Handbook of Liquid crystals. Vol. 1. Fundamentals*; Demus, D., Goodby, J., Gray, G. W., Spiess, H.-W., Vill, V., Eds.; Wiley-VCH: Weinheim, Germany, 1998; pp 189−203.

(32) Hansen, W. N. *J. Opt. Soc. Am.* **1968**, *58*, 380.

(33) Braudez, D.; Buffetau, T.; Desbat, B.; Fournier, P.; Ritcey, A.; Pezolet, M. *J. Phys. Chem. B* **1998**, *102*, 99.

(34) Kitaigorodskii, A. I. *Organic Chemical Crystallography*; Consultants Bureau: New York, 1961.

(35) Terrill, R. H.; Tanzer, T. A.; Bohn, P. W. *Langmuir* **1998**, *14*, 845.

assembled (the average tilt angle is of 52°), which is in accord with the results of the qualitative analysis of the IRRAS spectra (vide supra). Here, it is worth noting that for the DA adsorbed in liquidlike state at 2×10^{-5} M, $(A_{as}/A_s)_s \approx 1.1$ (Table 3) are less than $k_{max,as}/k_{max,s} = 1.3$ for bulk DA. Comparing these values with $k_{max,as}/k_{max,s} = 1.5$ measured for bulk HA and the value of 2.0 reported[36,37] for highly ordered bulk *n*-alkanes, one can arrive at the conclusion that a decrease in the ratio of the intensities of the $\nu_{as}(CH_2)$ and $\nu_s(CH_2)$ bands in the spectra of bulk samples as well as in the spectra of uniaxial and isotropic films originates from increasing disorder in the chain packing.

We roughly estimated the quantity of the adsorbed amines using $k_{max} = 1.04$ of hydrocarbon chains in a well-packed Langmuir−Blodgett film[21,33] for HA and $k_{max} = 0.62$ of hydrocarbon chains in a liquid state[38] for DA. The results are shown in Table 3. As would be expected, at almost the same coverage (ca. 0.8 monolayer) the chains of the adsorbed HAs are well organized (in a perpendicular hexagonal subcell) while those of DA are almost totally disordered.

ζ Potential and Flotation. In contrast to the case of quartz,[13] the ζ potential curves, having the similar general trends, do not follow the corresponding A_n curves at concentrations above the points of the charge reversal (pcr) (Figures 6 and 7). However, as in the case of quartz, the quantity of the adsorbed C_{12} and C_{16} amines at the pcrs is different. Since at the pcrs the 3D precipitation already takes place,[13] these facts can be attributed to the high heterogeneity of the particle surface at $C_b >$ pcr, where the surface contains bare sites along with patches covered by the highly organized 2D precipitates, the randomized 3D precipitates, and the bare surfaces. Each type of the surface patches is characterized by its own local pH and dissociation state, which determines the net particle charge. Due to a lower solubility limit, the quantity of HA precipitated at pcr is higher than that of DA. For the adsorbed amines of the same chain length, the relative areas covered by the 2D and 3D precipitates depend on the counterion, which gives the observed difference between the values of ζ potential.

Reproducing the well-known dependence of the flotability on the chain length of the primary amines,[39] the results of flotation with the HA appear to be independent of the origin of the amine counterion but DAAc seems to give a higher yield than DACl, the other things being the same. Since the role of the counterion in the adsorption of the amines is not understood yet, we only restrict ourselves to underlining this fact.

Discussion

Taken together, the spectroscopic results indicate that at low concentration the adsorbed species are the ammonium cations which are H-bonded to the surface and whose hydrocarbon chains are totally disordered. At a concentration higher than a critical concentration the neutral amine appears at the surface, inducing assembling of the hydrocarbon chains in the 2D space. When the concentration of the amines at the interface becomes greater than the saturation concentration, the ordinary 3D (bulk) precipitates appear at the surface. Each of these two-phase transitions at the interface is accompanied by increasing H-bonding strength of the amino (ammonium) groups to the surface and increasing density of the adsorbed film. Homogeneity of the monolayer is controlled by the surface homogeneity.

Qualitative identity of the above picture to that observed for quartz[13] we regard as a testimony of validity of the 2D−3D precipitation model for interpreting the mechanism of adsorption of weak-electrolyte-type surfactants on silicates. However, there are some differences, which should be discussed.

For all the amines, the C_{2D} values are lower for albite than for quartz: for DAs $C_{2D} = 1 \times 10^{-4}$ M and 2×10^{-5} M, and for HAs $C_{2D} = 2 \times 10^{-5}$ M and 3×10^{-6} M for quartz and albite, respectively. Since at pH 6.5 the minerals in question have almost the same initial ζ potentials (-33 ± 2 mV), this observation is inconsistent with the hemimicelle model which considers the electrostatic and hydrophobic interactions to be the dominant driven forces of the adsorption. As the same time, within the framework of the 2D−3D precipitation model, the difference in the C_{2D} values can be explained by the following facts. A comparison of the XPS N1s spectra of HAAc adsorbed on the fracture and powder surface (the last two lines in Table 1) shows that the relative and absolute content of the neutral form is higher in the case of the powder than that for the fracture surface conditioned even at the 10-fold higher concentration. The similar behavior was observed for quartz.[13] It follows that the formation of neutral amines, being closely related to the density and adsorption activity of the surface sites, is more favored on a more energetic surface. The albite sample has a higher specific surface area (2.78 m^2/g) as compared to that of quartz (1.30 m^2/g) and, hence, a higher density of the surface sites, which implies 2D precipitation to take place at a lower concentration. Next, the "H-bonded" band of the amines adsorbed at $C_b < C_{2D}$ (i.e., before the break) on quartz is positioned at remarkably higher frequencies than that for albite. In the case of quartz the band frequencies are 3270 (DAs) and 3120 cm^{-1} (HAs), while for albite the frequencies are 3150 cm^{-1} (DAs), 3000 cm^{-1} (HACl), and 2920 cm^{-1} (HAAc). According to the experimental[40] and theoretical[14] data, the substitution of an Al^{3+} for an Si^{4+} in a second-nearest-neighbor site increases proton affinity of the surface OH groups of silicates, while the charge balancing Na^+ ions affect this characteristic in the opposite direction. Since the albite surface conditioned in water is depleted with Na^+ ions, which may not be completely substituted by protons, it is possible that the surface silanols on albite bear a higher electron density and, therefore, are stronger acceptors of proton than the silanols on quartz. Moreover, as follows from the analysis of the BEs of the singlets in the XPS spectra, the adsorption on the sodium-cation vacancies is rather probable in the case of albite. The strengthening of H-bonding gives an additional contribution to decreasing the value of C_{2D} for albite. This interpretation testifies that before the break the adsorbed amines, acting as proton donors, are H-bonded and/or coordinated to the surface silanols.

The first monolayer of HAs at the (002) plane of quartz has biaxial anisotropy with the hydrocarbon chains inclined by 30° from the surface normal, while in the case of albite the layer is uniaxial and the chains are oriented perpendicular to the surface. The reason for this difference is different distances and arrangement of adsorption sites on the substrates employed. The effect of interplay of headgroup size−distance between adsorption sites on the

(36) Snyder, R. G. *J. Mol. Spectrosc.* **1961**, *7*, 116.
(37) Tasumi, M.; Shimanouchi T. *J. Chem. Phys.* **1965**, *43*, 1245.
(38) Hasegawa, T.; Takeda, S.; Kawaguchi, A.; Umemura, J. *Langmuir* **1995**, *11*, 1236.
(39) Somasundaran, P.; Healy, Th. W.; Fuerstenau, D. W. *J. Phys. Chem.* **1964**, *68*, 3562.
(40) Gil, B.; Broclawik, E.; Datka, J.; Klinowski, J. *J. Phys. Chem.* **1994**, *98*, 930.

chain orientation previously has been reported for self-assembled monolayers.[41,42]

The concentration of the second shift of the "H-bonded" band appears to be independent of the substrate: 4×10^{-5} M for HAs and 5×10^{-4} M for DAs. Moreover, the band positions after the second shift are the same (2830 $\pm$ 10 cm^{-1} for HA and 2950 $\pm$ 10 cm^{-1} for DA). It follows that the packing of the film adsorbed at concentration above the concentration of the second shift is also independent of the substrate. Both these facts are adequate with the concept of 3D precipitation. The latter process also explains the observed increase in both packing and isotropy of the adsorbed layer with increasing the layer thickness above one conventional monolayer. In contrast, the increase in both packing and isotropy in the multilayer films cannot be interpreted using either the hemimicelle model[6,7] or the condensation theory of Cases et al.[10,11] According to these theories, after monolayer coverage, a second uniform monolayer forms with the hydrocarbon tails oriented toward the surface and the charged amine heads toward the solution, which implies similar orientation of the hydrocarbon chains.

Conclusions

The results obtained using FTIR and XPS spectroscopy, ζ potential measurements, and flotation tests show that the mechanism of adsorption of long-chain amines at pH 6−7 onto albite and quartz is the successive 2D−3D precipitation (Figure 1). At concentration below C_{2D} ammonium cations are adsorbed sporadically while the hydrocarbon chains are oriented in all directions. As contrast to the case of quartz, adsorption on the sodiun vacancies can take place at this step. The break in the adsorption characteristics at C_{2D} is caused by the 2D precipitation of the neutral amine. From this concentration until the concentration of the bulk precipitation, C_{3D}, the adsorption increases due to increasing the packing density. At a polycrystalline albite surface, the chains are packed in a perpendicular hexagonal subcell, which differs from the packing mode on quartz. At these two steps, in addition to the electrostatic attractions and repulsions, H-bonding of amine/ammonium headgroups to surface silanols is important. Stronger H-bonds and a higher density of adsorption sites on albite cause the lower value of C_{2D} for albite as compared to that for quartz. At $C_b > C_{3D}$, randomly oriented well-packed 3D precipitates appear at the surface, decreasing its hydrophobicity. Coadsorption of the counterion was not revealed, but the counterion was found to affect indirectly the adsorption of the amines at concentrations above C_{3D}.

Acknowledgment. I.V.C. gratefully acknowledges the financial support of The Swedish Institute, Stockholm.

LA001023U

(41) Tao, Y.; Lee, M. *Thin Solid Films* **1994**, *244*, 810.
(42) Chechik, V.; Schönherr, H.; Vancso, G. J.; Stirling, C. J. M. *Langmuir* **1998**, *14*, 3003.